Trans- and *Cis*-Water Reactivities in d^6 Octahedral Ruthenium(II) Pentaaqua Complexes: Experimental and Density Functional Theory Studies[1,2]

Nicolas Aebischer,[†] Elena Sidorenkova,[‡] Mauro Ravera,[§] Gábor Laurenczy,[†] Domenico Osella,[§] Jacques Weber,*[,‡] and André E. Merbach*[,†]

Institut de Chimie Minérale et Analytique, Université de Lausanne, BCH-Dorigny, CH-1015 Lausanne, Switzerland, Département de Chimie Physique, Université de Genève, 30, quai Ernest Ansermet, CH-1211 Genève, Switzerland, and Dipartimento di Chimica Inorganica, Chimica Fisica e Chimica dei Materiali, Università di Torino, Via P. Giuria 7, I-10125 Torino, Italy

Received June 26, 1997[⊗]

The hexaaqua complex of ruthenium(II) represents an ideal starting material for the synthesis of isostructural compounds with a $[Ru(H_2O\text{-}ax)(H_2O\text{-}eq)_4L]^{2+}$ general formula. We have studied a series of complexes, where L = H_2O, MeCN, Me_2SO, $H_2C{=}CH_2$, CO, and $F_2C{=}CH_2$. We have evaluated the effect of L on the cyclic voltammetric response, on the rate and mechanism of exchange reaction of the water molecules, and on the structures calculated with the density functional theory (DFT). As expected, the formal redox potential, $E^{\circ\prime}(+2/+3)$, increases with the π-accepting capabilities of the ligands. For L = N_2, the oxidation to Ru(III) is followed by a fast substitution of dinitrogen by a solvent molecule, revealing the poor stability of the Ru(III)−N_2 bond. The water exchange reactions have been followed by ^{17}O NMR spectroscopy. The variable-pressure and variable-temperature kinetic studies made on selected examples are all in accordance with a dissociative activation mode for exchange. The positive activation volumes obtained for the axial and equatorial water exchange reactions on $[Ru(H_2O)_5(H_2C{=}CH_2)]^{2+}$ ($\Delta V_{ax}^{\ddagger}$ and $\Delta V_{eq}^{\ddagger} = +6.5 \pm 0.5$ and $+6.1 \pm 0.2$ cm^3 mol^{-1}) are the strongest evidence of this conclusion. The increasing *cis*-effect series was established according to the lability of the equatorial water molecules and is as follows: $F_2C{=}CH_2 \cong CO < Me_2SO < N_2 < H_2C{=}CH_2 < MeCN < H_2O$. The increase of the lability is accompanied by a decrease of the $E^{\circ\prime}$ values, but no change was found in the calculated Ru−H_2O_{eq} bond lengths. The increasing *trans*-effect series, established from the lability of the axial water molecule, is the following: $N_2 \ll MeCN < H_2O < CO < Me_2SO < H_2C{=}CH_2 < F_2C{=}CH_2$. A variation of the Ru−$H_2O_{ax}$ bond lengths is observed in the calculated structures. However, the best correlation is found between the lability and the calculated Ru−H_2O_{ax} bond energies. It appears, also, that a decrease of the electronic density along the Ru−O_{ax} bond and the increase of the lability can be related to an increase of the π-accepting capability of the ligand. For L = N_2, the calculations have shown that the Ru(II)−N_2 bond is weak. Consequently, the water exchange reaction proceeds through a different mechanism, where first the N_2 ligand is substituted by one water molecule to produce the hexaaqua complex of Ru(II). The water exchange takes place on this compound before re-formation of the $[Ru(H_2O)_5N_2]^{2+}$ complex.

Introduction

Interest in aqua complexes of ruthenium(II) has increased over the past few years.

First, from a synthetic viewpoint, ruthenium(II) shows as an ideal compromise between "softness and acidity" of complexed water and back-bonding into π^* orbitals of carbon π ligands.[3] This property allows us to envisage promising research in organometallic chemistry of Ru(II) in water. $[Ru(H_2O)_6](tos)_2$[4] is an ideal starting material for a series of new aqua complexes with ligands as varied as N-heterocycles, phosphines, THF,[5] arenes, and olefins[6] and for the facile syntheses of $[Ru(H_2O)_5L]^{2+}$ (L = N_2,[7] CO,[8] $H_2C{=}CH_2$[9]).

Second, Ru(II) aqua complexes are key intermediates in the metabolic processes associated with the antitumor activity of Ru(II) and Ru(III) compounds.[10,11] Ru(II) aqua complexes have also an important catalytic activity for the polymerization[12,13] and the isomerization of olefins.[14] In the ring-opening metathesis polymerization of some 7-oxanorbornenes derivatives, it was proposed that the catalyst was the olefinic monocomplex $[Ru(H_2O)_5(7\text{-oxanorbornene})]^{2+}$, formed in situ during the reaction.[12]

In order to understand what governs the reactivity of the

[†] Université de Lausanne.
[‡] Université de Genève.
[§] Università di Torino.
[⊗] Abstract published in *Advance ACS Abstracts*, December 1, 1997.

(1) High-Pressure NMR Kinetics. 84. For part 83, see ref 2.
(2) Bleuzen, A.; Pittet, P.-A.; Helm, L.; Merbach, A. E. *Magn. Reson. Chem.*, in press.
(3) Kölle, U. *Coord. Chem. Rev.* **1994**, *134*/*135*, 623.
(4) Bernhard, P.; Bürgi, H.-B.; Hauser, J.; Lehmann, H.; Ludi, A. *Inorg. Chem.* **1982**, *21*, 3936.
(5) (a) Bernhard, P.; Lehmann, H.; Ludi, A. *J. Chem. Soc., Chem. Commun.* **1981**, 1216. (b) Bailey, O. H.; Ludi, A. *Inorg. Chem.* **1985**, *24*, 2582. (c) Röthlisberger-Stebler, M.; Hummel, W.; Pittet, P.-A.; Bürgi, H.-B.; Ludi, A.; Merbach, A. E. *Inorg. Chem.* **1988**, *27*, 1358.
(6) (a) Kölle, U.; Flunkert, G.; Görissen, R.; Schmidt, M. U.; Englert, U. *Angew. Chem., Int. Ed. Engl.* **1992**, *31*, 440. (b) McGrath, D. V.; Grubbs, R. H. *J. Am. Chem. Soc.* **1991**, *113*, 3611.
(7) Laurenczy, G.; Helm, L.; Ludi, A.; Merbach, A. E. *Inorg. Chim. Acta* **1991**, *189*, 131.
(8) Laurenczy, G.; Helm, L.; Ludi, A.; Merbach, A. E. *Helv. Chim. Acta* **1991**, *74*, 1236.
(9) Laurenczy, G.; Merbach, A. E. *J. Chem. Soc., Chem. Commun.* **1993**, 187.
(10) *Metal Complexes in Cancer Chemotherapy*; Keppler, B. K., Ed.; VCH: Weinheim, Germany, 1993; pp 129−220.
(11) Alessio, E.; Mestroni, G.; Nardin, G.; Attia, W. M.; Calligaris, M.; Sava, G.; Zorzet, S. *Inorg. Chem.* **1988**, *27*, 4099.
(12) Novak, B. M.; Grubbs, R. H. *J. Am. Chem. Soc.* **1988**, *110*, 7542.
(13) France, M. B.; Grubbs, R. H.; McGrath, D. V.; Paciello, R. A. *Macromolecules* **1993**, *26*, 4742.
(14) Karlen, T.; Ludi, A. *Helv. Chim. Acta* **1992**, *75*, 1604.

S0020-1669(97)00783-0 CCC: $14.00

ligands in the first coordination sphere of the Ru(II) center, we have studied the effect of L (L: H_2O, **1**; MeCN, **2**; Me_2SO, **3**; $H_2C{=}CH_2$, **4**; CO, **5**; $F_2C{=}CH_2$, **6**; N_2, **7**) on the redox potentials of $[Ru(H_2O)_5L]^{2+}$ and rate of exchange of the bound water molecules at the axial (or *trans*) and equatorial (*cis*) positions. In addition, we have performed variable-pressure experiments on the ethylene complex, to determine the activation volumes of the water exchange reactions and to observe the effect of the bound ligand.

The *cis* and *trans* effects have been widely discussed in the case of square-planar complexes,[15] but are less understood for an octahedral geometry. The complexes listed above are ideal to study the *trans* and *cis* effects of a ligand L on the lability of σ-donating ligands like water. As the ligands in the equatorial plane are always identical along the series, they will play a negligible role in the kinetic effects. To have a deeper understanding of the experimental kinetic observations, computer calculations using the density functional theory (DFT) have been performed for **1**, **4**, **5**, and **7**, where the geometries were optimized and bond energies and orbital energies were calculated.

Experimental Section

Chemicals and Solutions. $[Ru(H_2O)_6](tos)_2$ ($tos^- = p$-toluenesulfonate anion) was prepared[16] and recrystallized from an aqueous solution of 1.2 M *p*-toluenesulfonic acid (Htos). Dimethyl sulfoxide (Fluka, p.a.), acetonitrile (Fluka, p.a.), carbon monoxide (Carbagas, 99.97%), ethylene (Carbagas, 99.95%), dinitrogen (Carbagas, 99.995%), and 1,1-difluoroethylene (Fluka, puriss., 99%) were used without further purification. All solutions were prepared in a glovebox ($O_2 < 2$ ppm). Water was deoxygenated using an argon stream before use, and all the kinetic runs were performed in the absence of O_2. The ^1H (^{13}C) NMR chemical shifts are referenced to TMS and measured with respect to the methyl protons (methyl carbon) of tos^-, $\delta = 2.38$ ppm (22.9 ppm). The ^{17}O NMR chemical shifts are referenced to bulk water ($\delta = 0$ ppm). The solvent for the ^1H and ^{13}C NMR characterization was 99.95% deuterated water. For the ^{17}O NMR measurements, doubly distilled water and 7−10% oxygen-17-enriched water (Yeda) were used.

Preparation of the Complexes of the Form $[Ru(H_2O)_5L](tos)_2$. The complexes **5**,[8] **7**[7], and **4**[9] were synthesized by following published procedures.

$[Ru(H_2O)_5(Me_2SO)](tos)_2$. **3** was prepared by dissolving in water 0.307 g of $[Ru(H_2O)_6](tos)_2$ and 0.048 g of Me_2SO and stirring the solution overnight at 35 °C. The end of the reaction was controlled by ^{17}O NMR. The solvent and the slight excess of Me_2SO were removed by vacuum distillation, and the product was dried overnight under a vacuum of 10^{-4} bar to give a yellow-brown powder. Anal. Calcd for $[Ru(H_2O)_5Me_2SO](C_7H_7O_3S)_2$: Ru, 16.52; C, 31.42; O, 31.39; H, 4.94; S, 15.72. Found: Ru, 16.70; C, 31.17; O, 31.65; H, 5.12; S, 15.52. ^{17}O NMR (54.24 MHz, $H_2{}^{17}O$): δ −164 (equatorial water), −58 (axial water).

$[Ru(H_2O)_5(F_2C{=}CH_2)](tos)_2$. In a sapphire NMR tube (which can support pressure up to 100 bars)[17] containing 2.5 g of degassed water was dissolved 0.304 g of $[Ru(H_2O)_6](tos)_2$. The resulting purple solution was then pressurized under 35 bars of 1,1-difluoroethylene and shaken for 60 h at 30 °C. After the gas pressure was removed, the water was evaporated under vacuum and the yellow-brown powder was dried under 10^{-4} bars overnight. Anal. Calcd for $[Ru(H_2O)_5(C_2H_2F_2)](C_7H_7O_3S)_2$: Ru, 16.91; C, 32.16; H, 4.39; S, 10.73; F, 6.36. Found: Ru, 16.75; C, 32.02; H, 4.26; S, 10.88; F, 6.26. ^1H NMR (400 MHz, D_2O): δ 4.24 (t, CH_2, $^3J_{HF} = 9.7$ Hz). ^{13}C NMR (100.62 MHz, D_2O): δ 165 (t, CF_2, $^1J_{CF} = 298$ Hz), 23.2 (tt, CH_2, $^1J_{CH} = 167$ Hz, $^2J_{CF} = 6$ Hz). ^{17}O NMR (54.24 MHz, $H_2{}^{17}O$): δ −147 (equatorial water), −31 (axial water).

$[Ru(H_2O)_5MeCN](tos)_2$. It was difficult to obtain this complex pure because the bis and tris complexes were produced as side products. To prevent their formation, solutions containing 0.1 mol kg^{-1} $[Ru(H_2O)_6]^{2+}$ and 0.06 mol kg^{-1} MeCN were prepared in water and heated at 40 °C to accelerate the reaction. The complete disappearance of the free acetonitrile was controlled by ^1H NMR. The water was then removed by vacuum distillation. ^{17}O NMR (54.24 MHz, $H_2{}^{17}O$): δ −192 (hexaaqua complex), −179 (equatorial water), −115 (axial water).

All the $[Ru(H_2O)_5L]^{2+}$ complexes can be synthesized with oxygen-17-enriched water by first dissolving $[Ru(H_2O)_6]^{2+}$ in enriched water and allowing the solution to stand $^1/_2$ h to reach isotopic equilibrium, before adding the ligand, L.

Electrochemical Measurements. These were performed using an EG&G PAR 273 electrochemical analyzer interfaced to a microcomputer, employing PAR M270 electrochemical software. A standard three-electrode cell was designed to allow the tip of the reference electrode (Ag/AgCl) to closely approach the working electrode. Positive-feedback *iR* compensation was applied. All measurements were carried out under argon in water; solutions were 1×10^{-3} M with respect to the compounds under study and 1×10^{-1} M with respect to the supporting electrolyte Htos. The temperature of the solution was kept constant within 1 °C. The working electrode was a Pt disk (diameter = 0.1 cm) sealed in soft glass which was polished with alumina followed by diamond paste. The electrode was then washed with distilled water and dried. This process yielded a reproducible surface for all experiments. The difference between the NHE and Ag/AgCl (reference electrode) is 0.197 V.

Kinetic Studies. All solutions used for the kinetic studies contained Htos (0.07−0.12 mol kg^{-1}) to prevent the formation of hydroxo species. The concentrations of the complexes were between 0.05 and 0.09 mol kg^{-1} ($I = 0.21$−0.39 mol kg^{-1}). The water exchange reactions were followed by ^{17}O NMR on a Bruker AM-400 spectrometer equipped with a 9.4 T wide-bore cryomagnet working at 54.2 MHz. The variable-temperature measurements were followed in a commercial thermostated probe, while the variable-pressure studies were performed up to 200 MPa by using a high-pressure probe.[18] The variable-temperature (pressure) ^{17}O NMR spectra were obtained using a 90° pulse length of 14 μs (12 μs) in the quadrature detection mode, with 2K data points resulting from 500−60 000 scans accumulated over a total spectral width of 50 kHz.

The solutions for the slow reactions ($k < 10^{-3}$ s^{-1}) were prepared at ambient temperature by dissolving the nonenriched (enriched) complex in enriched (nonenriched) water. The solutions were then transferred into the probe at measurement temperature. For faster reactions ($10^{-3} < k/s^{-1} < 0.4$), a fast-injection unit[19] was used. In this case, 100 scans were summed. For even faster reactions ($k^{298} > 1$ s^{-1}), the kinetics were followed by monitoring the broadening of the ^{17}O NMR signals. In this case, bulk water signal suppression and maximum excitation of the bound water signal was obtained by use of the "1, −3, 3, −1" pulse sequence.[20] At temperatures where the signals were adequately separated, the absence of significant effect of the above pulse sequence on the width of the signal of interest was checked. A line broadening (LB) of 5−10% of the line width at half-height, $\Delta\nu_{1/2}$, of the coordinated water signal was applied. The integrals and widths of the ^{17}O NMR signals were obtained by fitting a Lorentzian curve, and the transverse relaxation rate, $1/T_2{}^b$, was obtained from $\Delta\nu_{1/2}$ corrected for the LB by using the relation $1/T_2{}^b = \pi(\Delta\nu_{1/2} - \mathrm{LB})$. The temperature was measured by a substitution technique using a 100−Ω Pt resistor.[21]

The kinetic analysis was accomplished by a nonlinear least-squares fitting program. When differential equations were used, the mole fractions were calculated by integrating numerically the equations using the fourth-order Runge−Kutta method. The typical estimated precisions of the individual rate constants are 1−2% for the NMR measurements. The errors quoted are one standard deviation, but it is clear that due to

(15) Cattalini, L. In *Inorganic Reaction Mechanisms*; Edwards, J. O., Ed.; Wiley-Interscience: New York, 1970.
(16) Bernhard, P.; Biner, M.; Ludi, A. *Polyhedron* **1990**, *9*, 1095.
(17) Cusanelli, A.; Frey, U.; Richens, D. T.; Merbach, A. E. *J. Am. Chem. Soc.* **1996**, *118*, 5265.
(18) Frey, U.; Helm, L.; Merbach, A. E. *High Pressure Res.* **1990**, *2*, 237.
(19) Bernhard, P.; Helm, L.; Ludi, A.; Merbach, A. *J. Am. Chem. Soc.* **1985**, *107*, 312.
(20) Hore, P. J. *J. Magn. Reson.* **1983**, *55*, 283.
(21) Ammann, C.; Meier, P.; Merbach, A. E. *J. Magn. Reson.* **1982**, *46*, 319.

possible nonrandom errors, volumes of activation, $\Delta V^{\ddagger}$, can only be determined to within 1 cm^3 mol^{-1}.

Computational Details

The density functional theory (DFT) calculations were performed using two program packages: deMon, developed by Salahub *et al*.,[22] and the Amsterdam density functional (ADF) (2.0.1) package of Baerends *et al*.[23−25] Both the local density approximation (LDA) with the parametrization of Vosko, Wilk, and Nusair[26] and nonlocal density gradient (BP86) corrections to the exchange and correlation functionals due to Becke[27] and Perdew,[28] respectively, were used.

The deMon package is based on the implementation of the linear combination of Gaussian-type orbitals−density functional (LCGTO-MCP-DF) formalism.[29−31] The equilibrium geometries were obtained by applying the analytical expression for the LCGTO-DF energy gradients.[32] The "all-electron" Gaussian orbital basis set that was used is a 18s/12p/9d set contracted to (633321/53211*/531+) for ruthenium, a 9s/6p/1d set contracted to (5211/411/1) for carbon, nitrogen, and oxygen, and a 5s/1p set contracted to (41/1) for hydrogen.[33] The electron density and exchange-correlation potential were fitted using the following auxiliary bases: Ru(5,5; 5,5), C(5,2; 5,2), N(5,2; 5,2), O(5,2; 5,2), H(5,1; 5,1).

The ADF package is based on the use of Slater-type orbitals (STO), and for the 4s, 4p, 4d, 5s orbitals of ruthenium, 2s, 2p orbitals of carbon, nitrogen, and oxygen, and 1s orbital of hydrogen, an uncontracted triple-ζ STO basis set was employed. This basis set was augmented by a p diffuse function in the case of ruthenium and by a p polarization function in the case of hydrogen, whereas for the carbon, nitrogen, and oxygen atoms, an extra d polarization function was added. The inner cores of ruthenium (1s2s2p3s3p3d) as well as carbon (1s), nitrogen (1s), and oxygen (1s) were treated by the frozen-core approximation.[24] A set of auxiliary s, p, d, f, and g STO functions, centered on all nuclei, was used to fit the molecular density and represent the Coulomb and exchange potentials in each SCF cycle. The numerical integration procedure was developed by de Velde et al.[34]

In all the calculations, the accuracy of the total energies is 10^{-5} E_h. The SCF convergence criterion of gradient is 10^{-3}. The geometries of all complexes were fully optimized using the Broyden−Fletcher−Goldfarb−Shanna algorithm.

The reported binding energies were calculated using the deMon program and the formulas

$$E_{\text{binding}} = E([Ru(H_2O)_4L]^{2+}) + E(H_2O) - E([Ru(H_2O)_5L]^{2+}) \quad (1)$$

for Ru−H_2O_{axial} bonds and

$$E_{\text{binding}} = E([Ru(H_2O)_5]^{2+}) + E(L) - E([Ru(H_2O)_5L]^{2+}) \quad (2)$$

for Ru−L bonds, where L is H_2O, $H_2C{=}CH_2$, CO, or N_2. In eqs 1 and 2, $E(X)$ is the total energy of system X at the optimized geometry. The geometries of $[Ru(H_2O)_4(H_2C{=}CH_2)]^{2+}$, $[Ru(H_2O)_4CO]^{2+}$, and $[Ru(H_2O)_4N_2.]^{2+}$ were optimized under the constraint of C_{2v} symmetry using a square-pyramid structure. The basis set superposition error (BSSE) was corrected using the Boys−Bernardi technique.[35]

Atomic charges were derived from the Mulliken population analysis.[36] The MOLEKEL program package[37] was used to represent the molecular models, molecular orbitals, and electron densities of the species. All the calculations were performed on SGI workstations.

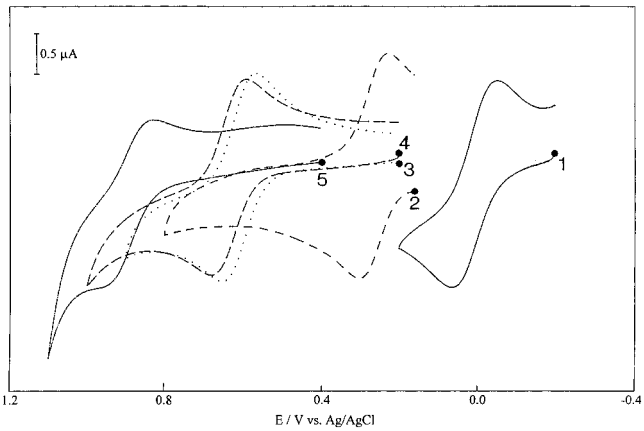

Figure 1. Cyclic voltammograms (0.2 V/s) of 10^{-3} M solutions of compounds **1**−**5** (see Results) in H_2O containing Htos (0.1 M) at a Pt working electrode; T = 298 K; • = starting potential.

Table 1. Electrochemical Parameters for $[Ru(H_2O)_5L](tos)_2$ Complexes 10^{-3} M in H_2O Containing Htos (0.1 M) at a Pt Working Electrode

ligand	no.	E_{su}[a]/ V vs NHE	$E^{\circ\prime}$ or E_p^a/ V vs NHE	ΔE_p or δE_p/ mV
H_2O	**1**	0.20	0.20[b]	60[b]
MeCN	**2**	0.46	0.46[b]	64[b]
Me_2SO	**3**	0.81	0.81[b]	70[b]
$H_2C{=}CH_2$	**4**	0.83	0.84[b]	90[b]
CO	**5**	1.09	1.10[b]	98[b]
$F_2C{=}CH_2$	**6**		1.16[c]	90[c]
N_2	**7**		0.92[c]	60[c]

[a] Summit potential, E_{su}, evaluated from the SWV response. [b] Chemically reversible processes for compounds **1**−**5**; $E^{\circ\prime} = (E_p^a + E_p^c)/2$; $\Delta E_p = E_p^a - E_p^c$. [c] Chemically irreversible processes for compounds **6** and **7**; E_p^a and $\delta E_p = E_p^a - E_{p/2}$ evaluated at 0.20 V s^{-1}.

Results

Electrochemical Measurements. Figure 1 shows the cyclic voltammograms (CV's) for aqueous solutions of compounds **1**−**5**, containing tosylic acid (Htos) as the supporting electrolyte (0.1 M) at a Pt electrode. The formal electrode potentials $E^{\circ\prime}$, evaluated as $(E_p^a + E_p^c)/2$ for chemically reversible processes (Figure 1) or the peak potential E_p, evaluated at a scan rate, υ, of 0.2 V s^{-1},[38] are summarized in Table 1.

Compounds **1**−**7** show a diffusion-controlled one-electron oxidation process as testified by the linearity of the plots of i_p^a vs $\upsilon^{1/2}$ and i_p^a vs concentration of the depolarizer, respectively. Compounds **1**−**5** exhibit chemically reversible processes since the i_p^c/i_p^a ratio is almost unity in the scan rate range 0.05−2.00 V s^{-1}; for **3** we observed a minor degree of chemical reversibility, (i.e., i_p^c/i_p^a ratio is 0.92 at 2.00 V s^{-1}). Compounds **6** and **7** show chemically irreversible processes since the

(22) Salahub, D. R.; Fournier, R.; Mlynarski, P.; Papai, I.; St.-Amant, A.; Ushio J. In *Density Functional Methods in Chemistry*; Labanowski, J. K., Andzelm, J. W., Eds.; Springer: New York, 1986; p 77.
(23) ADF. Department of Theoretical Chemistry, Vrije Universiteit, Amsterdam.
(24) Baerends, E. J.; Ellis, D. E.; Ros, P. *Chem. Phys.* **1973**, *2*, 41.
(25) Ziegler, T.; Rauk A. *Theor. Chim. Acta* **1977**, *49*, 143
(26) Vosko, S. H.; Wilk, L.; Nusair, M. *Can. J. Phys.* **1980**, *58*, 1200.
(27) Becke, A. D. *Phys. Rev. A* **1988**, *38*, 3098.
(28) Perdew, J. P *Phys. Rev. B* **1986**, *33*, 12, 8822.
(29) Sambe, H.; Felton, R. H. *J. Chem. Phys.* **1975**, *62*, 1122.
(30) Dunlap, B. I.; Connolly, J. W. D.; Sabin, J. R. *J. Chem. Phys.* **1979**, *71*, 3396.
(31) Andzelm, J.; Radzio, E.; Salahub, D. R. *J. Chem. Phys.* **1985**, *83*, 4573.
(32) Fournier, R.; Andzelm, J.; Salahub, D. R. *J. Chem. Phys.* **1989**, *90*, 6371.
(33) Godbout, N.; Salahub, D. R.; Andzelm, J.; Wimmer, E. *Can. J. Chem.* **1992**, *70*, 560.
(34) Te Velde, G.; Baerends, E. *J. Comput. Phys.* **1992**, *99*, 84.
(35) Boys, S. F.; Bernardi, F. *Mol. Phys.* **1970**, *19*, 553.
(36) Mulliken, R. S. *J. Chem. Phys.* **1955**, *23*, 1833, 1841, 2338, 2343.
(37) Flukiger, P. Ph.D. Thesis, University of Geneva, 1992; No. 2561.
(38) (a) Bard, A. J.; Faulkner, L. L. *Electrochemical Methods*; Wiley: New York, 1980. (b) Brown, E. R.; Sandifer, J. R. In *Physical Methods of Chemistry*; Rossiter, B. W., Hamilton, G. F., Eds.; Wiley: New York, 1986; Vol. II, Chapter IV. (c) Adams, R. N. *Electrochemistry at Solid Electrodes*; Marcel Dekker: New York, 1971. (d) Kissinger, P. T.; Heineman, W. R. *Laboratory Techniques in Electroanalytical Chemistry*; Marcel Dekker: New York, 1984.

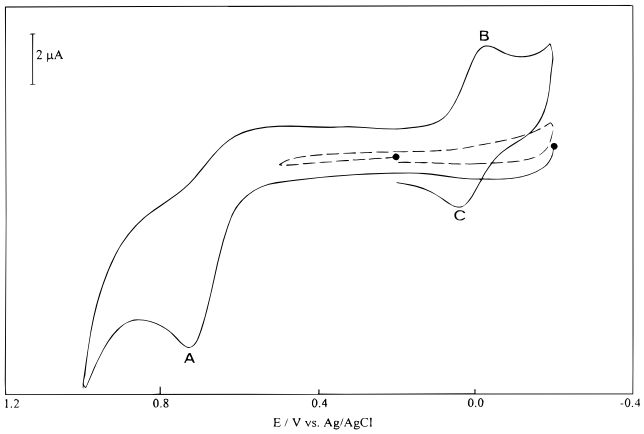

Figure 2. Cyclic voltammogram (0.2 V/s) of a 10^{-3} M solution of compound **7** in H_2O containing Htos (0.1 M) at a Pt working electrode; $T = 298$ K; • = starting potential.

associated cathodic peaks are totally absent and the slope derived from the plots of E_p^a vs log v is ca. 30 mV for the above scan rate range. Finally, all compounds show electrochemically reversible (fast electron transfer) or quasi-reversible processes as the $\Delta E_p = E_p^a - E_p^c$ values (evaluated for the chemically reversible processes of **1**−**5**) vary from 60 to 100 mV at 0.05 V s^{-1} and the $\delta E_p = E_p^a - E_{p/2}$ values (evaluated for the chemically irreversible processes of **6** and **7**) range from 60 to 80 mV at 0.05 V s^{-1}.

The data are consistent with a one electron-oxidation of Ru(II) to Ru(III).[38] A potential-controlled coulometric test on compound **1** confirms this stoichiometry. Finally, the square-wave voltammetric (SWV)[39] responses of **1**−**5** gave well-behaved oxidation peaks having summit potentials, E_{su},[40] consistent with the $E^{\circ\prime}$ data from the CV measurements (Table 1). The plots of i_{su} vs square root of frequency, in the range 30−120 Hz, are almost linear through the origin, and the peak widths, $W_{1/2}$, are independent of frequency and close to the values expected for a Nernstian one-electron process.[38] The electrochemical response of compound **7** (Figure 2) is also of interest. In the anodic scan, a chemically irreversible peak ($E_p(A) = +0.72$ V vs Ag/AgCl, scan rate 0.2 V s^{-1}) was obtained. In the reverse cathodic sweep ($E_\lambda = +1.00$ V), a chemically reversible redox couple (peaks B/C) was observed at a formal electrode potential identical to that of the aqueous complex **1**. This couple was not observed if the anodic sweep did not traverse peak A. Such behavior is best explained by a fast exchange of water for the coordinated N_2 molecule upon oxidation of the Ru metal center (Ru(II) → Ru(III)). To test this hypothesis, we employed a MeCN/H_2O solution (1:1 v/v) as the solvent. The CV response showed oxidation peak A at the same potential as in H_2O, but in the cathodic sweep two reversible couples, having almost the same peak heights, were observed. Their formal electrode potentials are very close to those of **1** and **2**, respectively. The electrochemical behavior of **7** is shown in Scheme 1.

Water Exchange on the $[Ru(H_2O)_5L]^{2+}$ Complexes. We have investigated the effect of the ligand, L, on the rate of exchange of the axial and equatorial water molecules. In Scheme 2, k_{ax} is the first-order rate constant for the exchange of the axial water molecule and k_{eq} is the first-order rate constant

Scheme 1. Proposed Mechanism for the Redox Behavior of $[Ru(H_2O)_5N_2](tos)_2$ (**7**)

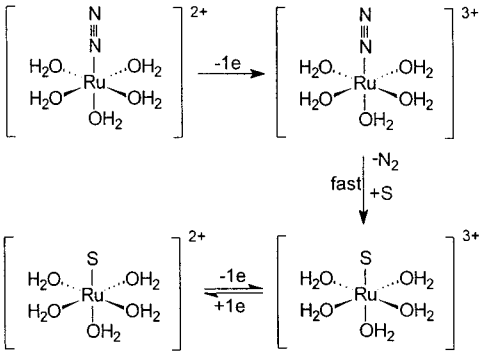

Scheme 2. Water Exchange Reactions at the Axial and Equatorial Positions in $[Ru(H_2O)_5L]^{2+}$

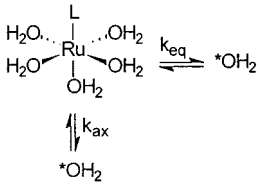

for the exchange of a particular equatorial water molecule.[41] This definition of the rate constant for the solvent exchange reactions has been extensively discussed.[42]

When, for a given monocomplex, k_{ax} and k_{eq} were sufficiently different (at least 2 orders of magnitude), both reactions were treated independently. Complexes **3**−**6** fall into this category. When the reaction was sufficiently slow enough ($k < 0.2$ s^{-1}), the exchange was monitored by following the evolution of the isotopic enrichment as a function of time. The rate law for the isotopic exchange can be expressed by eq 3, where x and x_∞

$$-\frac{dx}{dt} = k\frac{x - x_\infty}{1 - x_\infty} \tag{3}$$

represent the mole fractions of labeled water coordinated to the metal in a particular coordination site at the time of sampling and at exchange equilibrium, respectively. The experimental mole fraction was obtained according to eq 4, where $[H_2{}^{17}O]_c$

$$x = \frac{[H_2{}^{17}O]_c}{[H_2{}^{17}O]_c + [H_2{}^{17}O]_f} = \frac{I_c}{I_c + I_f} \tag{4}$$

and $[H_2{}^{17}O]_f$ are the concentrations of enriched water coordinated and enriched water in the bulk, respectively, and I are the integrals of the corresponding ^{17}O NMR signals. When the exchange takes place between only two sites, eq 3 can be integrated (eq 5). The exchange reactions of complexes **3** and

$$x = x_\infty + (x_0 - x_\infty)\exp\left(-\frac{kt}{1 - x_\infty}\right) \tag{5}$$

5 (axial and equatorial positions) and of complexes **4** and **6** (equatorial position) were analyzed using eq 5 (Table 2). For **3** and **4**, the water exchange in the equatorial position was also followed as a function of the temperature. The rate constants obtained using eq 3 at different temperatures were least-squares fitted to eq 6 with $\Delta H^\ddagger$ and $\Delta S^\ddagger$ as adjustable parameters. The

(39) (a) O'Dea, J.; Osteryoung, J.; Osteryoung, R. A. *Anal. Chem.* **1981**, *53*, 695. (b) Ramaley, L.; Krause, M. S., Jr. *Anal. Chem.* **1969**, *41*, 1362.

(40) The term summit current has been suggested for SWV by the IUPAC Commission on Electroanalytical Chemistry: Meites, L.; Zuman, O.; Nurnberg, H. W. *Pure Appl. Chem.* **1985**, *57*, 1491.

(41) Swaddle, T. W. *Adv. Inorg. Bioinorg. Mech.* **1983**, *2*, 95.

(42) Lincoln, S. F.; Merbach, A. E. *Adv. Inorg. Chem.* **1995**, *42*, 1.

(43) Ducommun, Y.; Newman, K. E.; Merbach, A. E. *Inorg. Chem.* **1980**, *19*, 3696.

Table 2. First-Order Rate Constants Obtained at Several Temperatures for Water Exchange at the Axial or Equatorial Position in $[Ru(H_2O)_5L]^{2+}$

L	site	[RuL]/mol kg^{-1}	[Htos]/mol kg^{-1}	I/mol kg^{-1}	T/K	k/s^{-1}
CO	axial	0.095	0.107	0.39	279.4	$(3.8 \pm 0.1) \times 10^{-3}$
	equatorial	0.095	0.107	0.39	298.0	$(2.87 \pm 0.02) \times 10^{-6}$
$F_2C{=}CH_2$	equatorial	0.073	0.102	0.32	308.4	$(9.3 \pm 0.2) \times 10^{-6}$
Me_2SO	axial	0.078	0.110	0.34	279.4	$(6.8 \pm 0.7) \times 10^{-2}$
	equatorial	0.080[a]	0.110	0.37	298.0	$(1.91 \pm 0.02) \times 10^{-5}$
	equatorial	0.083[a]	0.108	0.37	321.6	$(5.14 \pm 0.02) \times 10^{-4}$
	equatorial	0.081[a]	0.106	0.37	332.3	$(2.51 \pm 0.02) \times 10^{-3}$
	equatorial	0.092[b]	0.105	0.38	321.3	$(4.92 \pm 0.02) \times 10^{-4}$
$H_2C{=}CH_2$	equatorial	0.070[c]	0.110	0.33	279.0	$(1.54 \pm 0.01) \times 10^{-5}$
	equatorial	0.066[c]	0.120	0.32	298.0	$(2.28 \pm 0.02) \times 10^{-4}$
	equatorial	0.072	0.100	0.31	312.3	$(1.73 \pm 0.02) \times 10^{-3}$
	equatorial	0.050	0.070	0.22	322.0	$(1.00 \pm 0.02) \times 10^{-2}$

[a] Contains 8% $[Ru(H_2O)_6]^{2+}$. [b] Contains free Me_2SO dissolved in the solution, $[Me_2SO] = 0.540$ mol kg^{-1}. [c] Contains 4% $[Ru(H_2O)_6]^{2+}$.

Table 3. NMR and Kinetic Parameters Derived from Variable-Temperature and Variable-Pressure Studies for Water Exchange at the Axial or Equatorial Position in $[Ru(H_2O)_5L]^{2+}$

	L = Me_2SO	L = $H_2C{=}CH_2$		L = $F_2C{=}CH_2$
site	equatorial	axial	equatorial	axial
k^{298}/s^{-1}	$(1.9 \pm 0.3) \times 10^{-5}$	2.9 ± 0.8	$(2.8 \pm 0.3) \times 10^{-4}$	4.3 ± 1
$\Delta H_{ex}^{\ddagger}$/kJ mol^{-1}	112.9 ± 6	85.2 ± 4	106.6 ± 5	73.0 ± 3
$\Delta S_{ex}^{\ddagger}$/J K^{-1} mol^{-1}	$+43.2 \pm 17$	$+49.5 \pm 12$	$+44.6 \pm 18$	$+12.1 \pm 9$
$(1/T_{2Q}{}^{b})^{298}$/s^{-1}		511 ± 12		659 ± 10
$E_Q{}^{b}$/kJ mol^{-1}		22.8 ± 1		20.0 ± 0.7
$\Delta V_{ex}^{\ddagger}$/cm^3 mol^{-1}		$+6.5 \pm 0.5$[a]	$+6.1 \pm 0.2$[b]	
$k_{ex,0}{}^{T}$/s^{-1}		633 ± 11[a]	$(1.12 \pm 0.01) \times 10^{-4}$ [b]	
$\Delta V_Q^{\ddagger}$/cm^3 mol^{-1}		$+0.7 \pm 0.3$[a]		

[a] 354.8 K. [b] 292.8 K.

$$k = \frac{k_B T}{h} \exp\left(\frac{\Delta S^{\ddagger}}{R} - \frac{\Delta H^{\ddagger}}{RT}\right) \quad (6)$$

errors for the rate constants were obtained by repeating the fit with $k_{eq}{}^{298}$ and $\Delta H^{\ddagger}$ as adjustable parameters (Table 3). For **4**, the exchange at the equatorial position was also followed as a function of the pressure (Figure 3). The pressure dependence of ln k_{eq} can be described by eq 7 if we assume a pressure-

$$\ln k_{eq} = \ln k_{eq,0} - \frac{P\,\Delta V_{eq}{}^{\ddagger}}{RT} \quad (7)$$

independent $\Delta V_{eq}{}^{\ddagger}$, as is often observed for simple solvent-exchange reactions ($k_{ex,0}$ is the exchange rate constant at zero pressure).[43] The values obtained are reported in Table 3.

The water exchanges at the axial position for **4** and **6** were followed by monitoring the broadening of the ^{17}O NMR signal of the coordinated water molecule as a function of the temperature ($276 < T/K < 367$) (Figure 4). For a water molecule coordinated to a diamagnetic ion and in the case of slow exchange, the transverse relaxation rate, $1/T_2{}^{b}$, is the sum of the contribution of the quadrupolar relaxation, $1/T_{2Q}{}^{b}$, and of the first-order rate constant for the water exchange, k_{ex} (eq 8). The temperature dependence of k_{ex} is given by the Eyring

$$1/T_2{}^{b} = 1/T_{2Q}{}^{b} + k_{ex} \quad (8)$$

equation (eq 6), whereas an Arrhenius temperature dependence for the quadrupolar relaxation rate was assumed (eq 9), where

$$\frac{1}{T_{2Q}{}^{b}} = \left(\frac{1}{T_{2Q}{}^{b}}\right)^{298} \exp\left[\frac{E_Q{}^{b}}{R}\left(\frac{1}{T} - \frac{1}{298.15}\right)\right] \quad (9)$$

$(1/T_{2Q}{}^{b})^{298}$ is the quadrupolar relaxation rate at 298.15 K and $E_Q{}^{b}$ the corresponding activation energy. A combination of eqs 6, 8, and 9 was used to fit the experimental transverse relaxation rate obtained from the half-width of the ^{17}O NMR signal, $\Delta\nu_{1/2}$ (eq 10). The exchange and NMR parameters are listed in Table 3, and the experimental data and the calculated curves are illustrated in Figure 4.

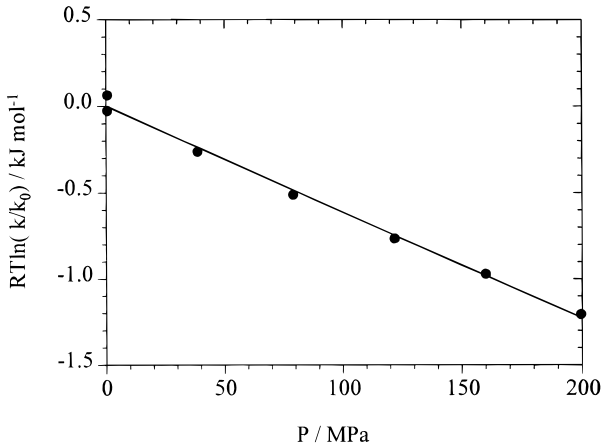

Figure 3. Plot of $RT \ln(k/k_0)$ vs pressure for the exchange of a particular water molecule at the equatorial position in $[Ru(H_2O)_5(H_2C{=}CH_2)]^{2+}$ at 292.8 K.

$$1/T_2{}^{b} = \pi\,\Delta\nu_{1/2} \quad (10)$$

The exchange of the axial water molecule in **4** was also followed as a function of the pressure (Table 4). Equation 7 was used to describe the variation of ln k_{ax} with the pressure and eq 11 to describe the variation of the quadrupolar relaxation

$$\ln\left(\frac{1}{T_{2Q}{}^{b}}\right) = \ln\left(\frac{1}{T_{2Q}{}^{b}}\right)_0 - \frac{P\,\Delta V_Q^{\ddagger}}{RT} \quad (11)$$

rate as a function of the pressure, where $(1/T_{2Q}{}^{b})_0$ is the contribution at zero pressure and $\Delta V_Q{}^{\ddagger}$ the quadrupolar activa-

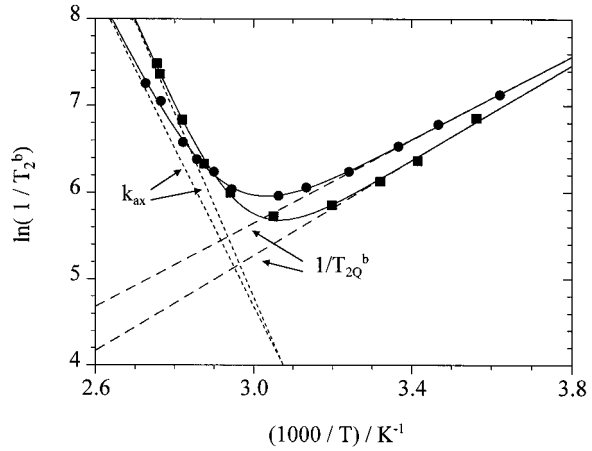

Figure 4. Temperature dependence of $1/T_2^b$ from the ^{17}O NMR signals of the axial water molecule in $[Ru(H_2O)_5(H_2C{=}CH_2)]^{2+}$ (■, [Ru] = 0.070 mol kg^{-1}, [Htos] = 0.110 mol kg^{-1}) and in $[Ru(H_2O)_5(F_2C{=}CH_2)]^{2+}$ (●, [Ru] = 0.073 mol kg^{-1}, [Htos] = 0.103 mol kg^{-1}).

Table 4. Effect of Pressure on the Tranverse Relaxation Rate of the ^{17}O NMR Signal of the Water Molecule Coordinated at the Axial Position in $[Ru(H_2O)_5(H_2C{=}CH_2)]^{2+}$ at Two Different Temperatures[a]

P/MPa	$1/T_2^b$(291.4 K)/s^{-1}	*P*/MPa	$1/T_2^b$(354.8 K)/s^{-1}
0.1	668	0.1	756
0.1	681	0.1	757
27.2	682	26.8	722
48.5	709	51.0	675
75.9	710	76.2	641
99.2	677	100.9	610
126.5	644	126.1	575
153.1	644	150.5	596
175.3	639	175.1	547
197.0	671	200.5	516

[a] $[Ru(H_2O)_5(H_2C{=}CH_2)^{2+}] = 0.0903$ mol kg^{-1}; [Htos] = 0.096 mol kg^{-1}.

Table 5. Derived NMR and Kinetic Parameters for the Variable-Pressure Study of Axial Water Exchange on $[Ru(H_2O)_5(H_2C{=}CH_2)]^{2+}$ in $D_2{}^{17}O$, 10 atom % Enriched in ^{17}O

T/K	$(1/T_{2Q}^b)_0$/s^{-1}	% $(1/T_{2Q}^b)_0$[a]	$k_{ax,0}$/s^{-1}	% $(k_{ax,0})$[a]
291.4	688 ± 10	99.8	{1.3}	0.2
354.8	{117.5}	12.5	633 ± 11	87.5

[a] Each contribution is expressed as a percentage of the value of $1/T_2^b$ as obtained from the variable-temperature measurements. The values in braces were fixed during the fitting procedure.

tion volume. The variable-pressure $1/T_2^b$ measurements were performed at two different temperatures (*T*/K = 291.4 and 354.8) in order to separate the pressure effects on the quadrupolar relaxation and the chemical exchange. In theory, $k_{ax,0}$ and $(1/T_{2Q}^b)_0$ at each temperature could be fixed at the values obtained from the variable-temperature analysis. However, in practice small differences in temperature calibration between the variable-temperature and variable-pressure experiments could cause nonrandom errors in the $1/T_2^b$ measurements. Therefore, at each temperature we fixed only the parameter ($k_{ax,0}$ or $(1/T_{2Q}^b)_0$) which contributed least to the magnitude of $1/T_2^b$. The other parameters $(1/T_{2Q}^b)_0^{298.4}$, $k_{ax,0}^{354.8}$, $\Delta V_{ax}^{\ddagger}$, and $\Delta V_Q^{\ddagger}$ were used as adjustable parameters to fit the experimental relaxation rate as a function of the pressure by eqs 7, 8, and 11. The $k_{ax,0}$ and $(1/T_{2Q}^b)_0$ values (fixed and fitted) are reported in Table 5, and the corresponding activation volumes are given in Table 3.

When k_{ax} and k_{eq} are of the same order of magnitude for a given complex, eq 5 cannot be used. This is the case when the concentration of coordinated enriched water is not always negligible throughout the exchange reaction compared to the concentration of enriched water in the bulk. For example, when the monocomplex is enriched in ^{17}O prior to dissolving it into nonenriched water, both exchange reactions, between the two coordination sites and the bulk must be treated simultaneously. In the case of **2**, k_{ax} and k_{eq} are very similar. Moreover, this complex is synthesized with an excess of hexaaqua complex so at the end we have a mixture of **2** and **1** in solution. Consequently, exchange reactions of both complexes were treated simultaneously using eqs 12−15 (see Supporting Information for the development). x_{ax}, x_{eq}, x_{hex}, and x_S are the mole fractions of enriched water at the axial and equatorial positions in the monocomplex, enriched water coordinated in the hexaaqua complex, and enriched water in the bulk respectively; *q* and q_{hex} are the total concentrations of monocomplex and hexaaqua complex, respectively, divided by the total concentration of free water. The adjustable parameters were k_{ax}, k_{eq}, k_{ex}, *q*, and q_{hex}. The results obtained at three different temperatures are reported in Table 6 (an example fit is shown in Supporting Information Figure S3).

$$\frac{dx_{ax}}{dt} = -k_{ax}(x_{ax} - qx_S) \tag{12}$$

$$\frac{dx_{eq}}{dt} = -k_{eq}(x_{eq} - 4qx_S) \tag{13}$$

$$\frac{dx_{hex}}{dt} = -k_{ex}(x_{hex} - 6x_S q_{hex}) \tag{14}$$

$$x_S = 1 - x_{ax} - x_{eq} - x_{hex} \tag{15}$$

Another mechanism is proposed for the water exchange on **7** (Scheme 3). It implies that the Ru−N bond strength is weaker than the Ru−O bond strengths. Moreover, when the breaking of the Ru−N_2 bond is the rate-determining step, the rate constant for the exchange of the axial water molecule is the same as the one for the exchange of a particular equatorial water molecule. If the steady state hypothesis is made for the hexaaqua complex, eqs 16−19 (developed in the Supporting Information) describe

$$\frac{dx_{ax}}{dt} = -k_d x_{ax} + \frac{1}{6}k_f x_{hex}[L] \tag{16}$$

$$\frac{dx_{eq}}{dt} = -k_d x_{eq} + \frac{2}{3}k_f x_{hex}[L] \tag{17}$$

$$\frac{dx_{hex}}{dt} = k_d(x_{ax} + x_{eq} + qx_S) - k_f x_{hex}[L] + 6k_{ex}x_S\frac{qk_d}{k_f[L]} - k_{ex}x_{hex} \tag{18}$$

$$x_S = 1 - x_{ax} - x_{eq} - x_{hex} \tag{19}$$

the rate law for the water exchange reactions (Scheme 3). In these equations, the water exchange rate constant for **1**, k_{ex}, known from a previous study,[44] was fixed during the fitting procedure. It was shown that the monocomplex formation rate constant, k_f, does not depend on the nature of the incoming ligand[45] and was therefore also fixed. The mole fractions of enriched water in the different sites were calculated by integrat-

(44) Rapaport, I.; Helm, L.; Merbach, A. E.; Bernhard, P.; Ludi, A. *Inorg. Chem.* **1988**, *27*, 873.
(45) Aebischer, N.; Laurenczy, G.; Ludi, A.; Merbach, A. E. *Inorg. Chem.* **1993**, *32*, 2810.

Table 6. Derived Kinetic Parameters Obtained at Three Different Temperatures for Water Exchange Reactions in Water Solutions of a Mixture of $[Ru(H_2O)_5MeCN]^{2+}$ and $[Ru(H_2O)_6]^{2+}$

T/K	279.0	279.3	297.8
$[Ru(H_2O)_5MeCN^{2+}]$/mol kg^{-1}	0.023	0.054	0.038
$[Ru(H_2O)_6{}^{2+}]$/mol kg^{-1}	0.022	0.010	0.031
[Htos]/mol kg^{-1}	0.076	0.066	0.083
I/mol kg^{-1}	0.21	0.26	0.29
k_{ex}/s^{-1}	$(8.8 \pm 0.3) \times 10^{-4}$	$(8.0 \pm 0.3) \times 10^{-4}$	$(1.86 \pm 0.05) \times 10^{-2}$
k_{ax}/s^{-1}	$(3.9 \pm 0.5) \times 10^{-4}$	$(4.6 \pm 0.2) \times 10^{-4}$	$(7.2 \pm 0.7) \times 10^{-3}$
k_{eq}/s^{-1}	$(8.5 \pm 0.4) \times 10^{-5}$	$(9.3 \pm 0.1) \times 10^{-5}$	$(1.46 \pm 0.03) \times 10^{-3}$
q	$(4.03 \pm 0.07) \times 10^{-4}$	$(1.06 \pm 0.03) \times 10^{-3}$	$(7.27 \pm 0.04) \times 10^{-4}$
q_{hex}	$(4.2 \pm 0.3) \times 10^{-4}$	$(2.2 \pm 0.1) \times 10^{-4}$	$(5.78 \pm 0.02) \times 10^{-4}$

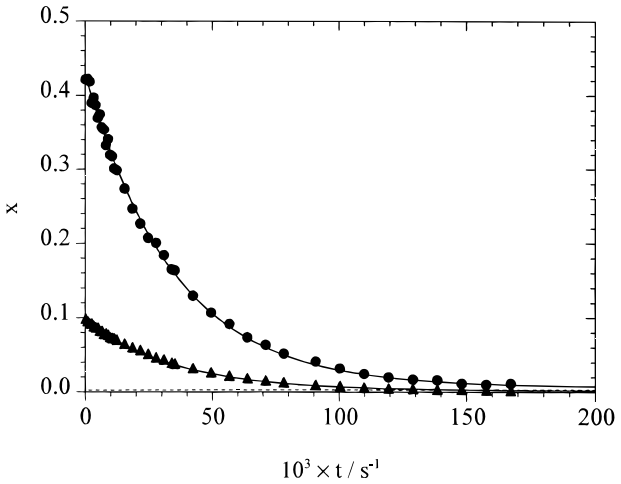

Figure 5. Evolution of the mole fractions of enriched water coordinated in the monocomplex $[Ru(H_2O)_5N_2]^{2+}$ at the axial (▲) and equatorial (●) positions as a function of time at 298.6 K under 6 MPa N_2 pressure and the calculated mole fraction of enriched water coordinated in $[Ru(H_2O)_6]^{2+}$ (- - -); [Ru] = 0.078 mol kg^{-1}, [Htos] = 0.101 mol kg^{-1}.

Scheme 3. Proposed Mechanism for the Water Exchange in the Monocomplex $[Ru(H_2O)_5N_2]^{2+}$

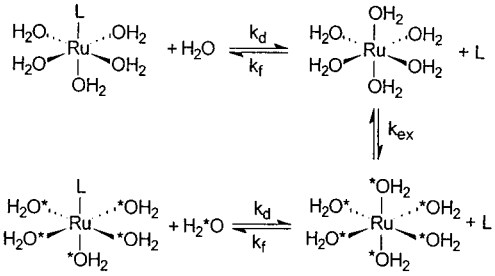

Table 7. Derived Kinetic Parameters Obtained at 298.6 K for the Water Exchange Reaction in the $[Ru(H_2O)_5N_2]^{2+}$ Complex Studied under 6 MPa Pressure of N_2 in a Sapphire NMR Tube[a]

$[N_2]$/mol kg^{-1}	{0.044}[b]	$x_{eq}(0)$	0.428 ± 0.001
k_f/mol^{-1} kg s^{-1}	$\{2.1 \times 10^{-3}\}$[c]	$x_{ax}(0)$	0.098 ± 0.001
k_{ex}/s^{-1}	$\{1.9 \times 10^{-2}\}$[d]	k_d/s^{-1}	$(2.88 \pm 0.02) \times 10^{-5}$
$x_{hex}(0)$	{0}	q	$(1.5 \pm 0.2) \times 10^{-3}$

[a] The parameters in braces were fixed during the fitting procedure; $[Ru(H_2O)_5N_22+]$ = 0.078 mol kg^{-1}, [Htos] = 0.101 mol kg^{-1}. [b] Reference 7. [c] Reference 45. [d] Reference 44.

ing numerically eqs 16−19 using the fourth-order Runge−Kutta method. An example of a fit is shown in Figure 5, and the results are reported in Table 7.

Computational Results and Discussion

Calculations of $[Ru(H_2O)_6]^{2+}$. Table 8 presents the results of DFT geometry optimizations of $[Ru(H_2O)_6]^{2+}$. This system was chosen as a test case for both LDA and BP86 calculations using both program packages. In addition, it is interesting to compare these DFT results with previous calculations performed using the *ab initio* SCF method.[46]

Table 8. Comparison of Experimental and Calculated Structures for the $[Ru(H_2O)_6]^{2+}$ Complex[a]

		deMon[c]		ADF[d]	
	exp[b]	LDA	BP86	LDA	BP86
d(Ru−O)	2.122	2.095	2.161	2.090	2.154
d(O−H)		0.983	0.980	0.976	0.973
∠HOH		109.5	108.5	110.4	109.4

[a] Distances in angstroms, angles in degrees. [b] Reference 4. [c] Calculated by assuming T_h symmetry. [d] Calculated by assuming D_{2h} symmetry, as no provision for T_h symmetry has been made in the ADF package.

It is seen that the two DFT programs lead to very similar results, the largest discrepancy being 0.007 Å for bond distances and 0.9° for bond angles. The increase in Ru−O bond distance upon going from LDA to BP86 approximations is a characteristic feature of DFT calculations performed for coordination compounds,[47,48] whereas the O−H bond length is practically insensitive to the level of the calculations. Therefore, when the calculated metal−oxygen distances are compared with the experimental values, it is seen that the LDA approximation leads to a too short a distance and the BP86 formalism to one that is too long. As the experimental distance is approximately equal to the average of LDA and BP86 values, there is apparently no reason to prefer one model to the other. However, as LDA calculations are significantly less demanding in computing time, we used this level of approximation and the deMon program package throughout this investigation. Finally, the comparison with the *ab initio* SCF method[46] shows that the Ru−O bond distance predicted in DFT is significantly shorter than the *ab initio* results (2.197 Å). This is not surprising, as it is well-known that *ab initio* calculations performed at the SCF level are frequently in error for metal−ligand bond lengths.[49]

The orbital energies and corresponding charge distributions of the upper valence molecular orbitals (MOs) of the ^1A_g $(2t_g)^6(1e_g)^0$ ground state of **1** are presented in Table 9 and some of their three-dimensional models in Figure 6. As expected for octahedral transition metal compounds, the calculated sequence of predominantly metal d orbitals is $2t_g(d\pi) < 2e_g(d\sigma)$ for this formally d^6 compound of Ru(II). The metal 4d contributions to these MOs are somewhat different: the σ^* antibonding $2e_g$ LUMO exhibits a larger delocalization on the ligands than the π^* $2t_g$ HOMO. Below the $2t_g$ HOMO, one finds the typically nonbonding $2t_u$ MO and, in sequence, the π bonding $1t_g$ MO, the nonbonding $1t_u$ MO, and the σ bonding $1e_g$ and $1a_g$ MOs. At a higher energy than the $2e_g$ LUMO, one finds $2a_g$, which is a typical Rydberg MO with Ru 5s character.

(46) Åkesson, R.; Pettersson, L. G. M.; Sandström, M.; Wahlgren, U. *J. Am. Chem. Soc.* **1994**, *116*, 8691.
(47) Sosa, C.; Andzelm, J.; Elkin, B. C.; Wimmer, E.; Dobbs, K. D.; Dixon, D. A. *J. Phys. Chem.* **1992**, *96*, 6630.
(48) Furet, E.; Weber, J. *Theor. Chim. Acta* **1995**, *91*, 157.
(49) Veillard, A. *Chem. Rev.* **1991**, *91*, 743.

Table 9. Ground-State Orbital Energies and Corresponding Charge Distribution[a] for the Upper Valence MOs of the $[Ru(H_2O)_6]^{2+}$ Complex (T_h Symmetry) Calculated According to LDA DFT Calculations

			charge distribution/%					
			Ru			O		H
orbital type	orbital energy/eV	occ[b]	s	p	d	s	p	s
$2a_g$	−9.14	0	61					39
$2e_g$	−10.42	0			74	5	11	10
$2t_g$	−12.58	6			87		10	3
$2t_u$	−16.64	6		1			96	3
$1t_g$	−16.94	6			10		87	3
$1t_u$	−19.31	6		1		8	78	13
$1e_g$	−20.40	4			20	5	64	11
$1a_g$	−20.51	2	8			5	75	12

[a] The calculation of the charge distribution was performed using a Mulliken population analysis. [b] Occupation number of each MO.

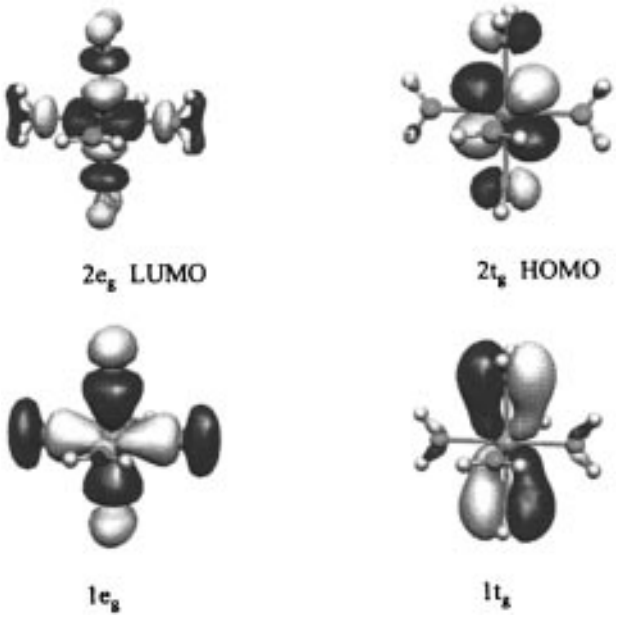

Figure 6. Three-dimensional models of some MOs of system **1**.

Calculations of $[Ru(H_2O)_5L]^{+2}$ Complexes (L = $H_2C{=}CH_2$, CO, N_2). Figure 7 presents the geometries calculated for **4**, **5**, and **7**. As the ethylene molecule in **4** is no longer planar (the dihedral angle between the two CH_2 groups is 154.3°) and the C−C bond exhibits a twist angle of 22.8° with respect to the Ru−O_{eq} bond, the symmetry of **4** at the optimized geometry is C_1. This is essentially in agreement with previously reported conformations of monoolefin transition metal complexes.[50] Complexes **5** and **7** were optimized by assuming C_{2v} symmetry; lowering to C_1 symmetry led to insignificant differences in the energies and structural parameters. The $O_{ax}RuO_{eq}$ angles in **4** (79.8, 80.0, 80.9, 95.9°), **5** (83.7, 83.7, 87.1, 87.1°), and **7** (84.4, 84.4, 88.5, 88.5°) decrease in the presence of the ligand L, which can probably be rationalized from a steric effect of the ligand L, as it is the largest for **4**.

We note that the C−C bond length increases by 0.075 Å in the monoolefin complex as compared with the free ethylene molecule. This significant C−C bond elongation may be interpreted by both a donation of π ethylene electrons to Ru and a back-donation from the metal to the π^* orbital of the olefin.

Complex **5** is characterized by a C−O bond length of 1.151 Å, which is slightly longer than that in uncomplexed carbon monoxide (1.140 Å), this effect being attributed to the π back-bonding donation from Ru to the π^* antibonding MO of CO. This result is in agreement with the slower stretching frequency of CO when bound to Ru(II).[8]

The end-on conformation of **7** was found to be more stable than the side-on one by 88.5 kJ mol^{-1}. In addition, the N−N bond length is elongated by 0.028 Å as compared with that of free N_2. In spite of the fact that CO and N_2 are isoelectronic molecules, the values of Ru−O_{ax} bond lengths in **5** and **7** are different, which can be explained in terms of their electronic structures (vide infra).

In this investigation we have chosen $[Ru(H_2O)_5L]^{2+}$ complexes having unsaturated ligands L (L = $H_2C{=}CH_2$, CO, N_2) with low-lying π^* orbitals. Indeed, these ligands are known to be good acceptors of electron density from the dπ orbitals of metals. It is then expected that the Ru−L bond energies will be larger for these ligands than for L = H_2O. This is confirmed in Table 10, which show that addition of π back-donation from dπ orbitals of Ru to the π^* orbital of L leads to an increase in the Ru−L bond energies. The molecular orbitals responsible for the corresponding π back-donation in complexes **4**, **5**, and **7** are presented in Figure 7. It is seen that for **4** there is an interaction of the π^* orbital of ethylene with the d_{xz} orbital of Ru only but in **5** there are two d interacting orbitals: d_{xz} and d_{yz}. This may explain the fact that the Ru−L bonding energy is larger for **5** than for **4** by 37.8 kJ mol^{-1}. There is no π back-bonding interaction found in **7**, which correlates with its Ru−L bonding energy being similar to that of **1**.

Effect of L on the Redox Potentials and the Chemical Shifts. Table 11 summarizes the thermodynamic and kinetic results. The redox potentials are higher for complexes containing ligands with π-accepting capabilities. Our experimental values can be compared with the calculated redox potential, E_{calc}, using Lever's parameters.[51] In this method, each ligand is assigned a parameter calculated from complexes with known redox potentials. These parameters are added, and the sum is introduced into an equation characteristic of the metal center in order to calculate the E_{calc} values. As can be seen, the experimental values are always more positive than the calculated ones. It appears that a π-accepting ligand, L, is more efficient in stabilizing Ru(II) versus Ru(III) when *trans* to a purely σ-donating ligand. This can be understood as in this case L does not share the d_{xz} or d_{yz} orbital of the metal with a ligand *trans* to it. To obtain more accurate calculated values, it may be more appropriate to separate the σ and π contributions of L to the parameters used to calculate the E_{calc} values. The calculated redox potential for **3** is particularly far from the experimental value. This is due to the fact that the Lever parameter was calculated for complexes where Me_2SO shows different binding modes, i.e. O- or S- bonded. It should be appropriate to define two values for Me_2SO, one for the O-bonded form and one for the S-bonded form.

Linear relationships between the natural logarithm of the absolute value of the ^{17}O NMR chemical shift of the coordinated water molecules and the redox potential, $E^{\circ\prime}$ values were observed: $\ln(|\delta_{ax}|) = -0.26(9)E^{\circ\prime} + 5.31(7)$, $R = 0.981$; $\ln(|\delta_{eq}|) = -2.01(9)E^{\circ\prime} + 5.64(7)$, $R = 0.985$ (δ_{ax} and δ_{eq} are the ^{17}O NMR chemical shifts of the axial and equatorial water molecules, respectively; see Table 11). **7** is the only complex that does not obey this relationship. This is expected because the electrochemical behavior of **7** is different (vide supra). Even if these two equations have no real physical meaning, they are interesting as they provide an easy way to estimate redox potentials for complexes of the type $[Ru(H_2O)_5L]^{2+}$. If we

(50) Albright, T. A.; Hoffmann, R.; Thibeault, J. C.; Thorn, D. L *J. Am. Chem. Soc.* **1979**, *111*, 3801.

(51) Lever, A. B. P. *Inorg. Chem.* **1990**, *29*, 1271.

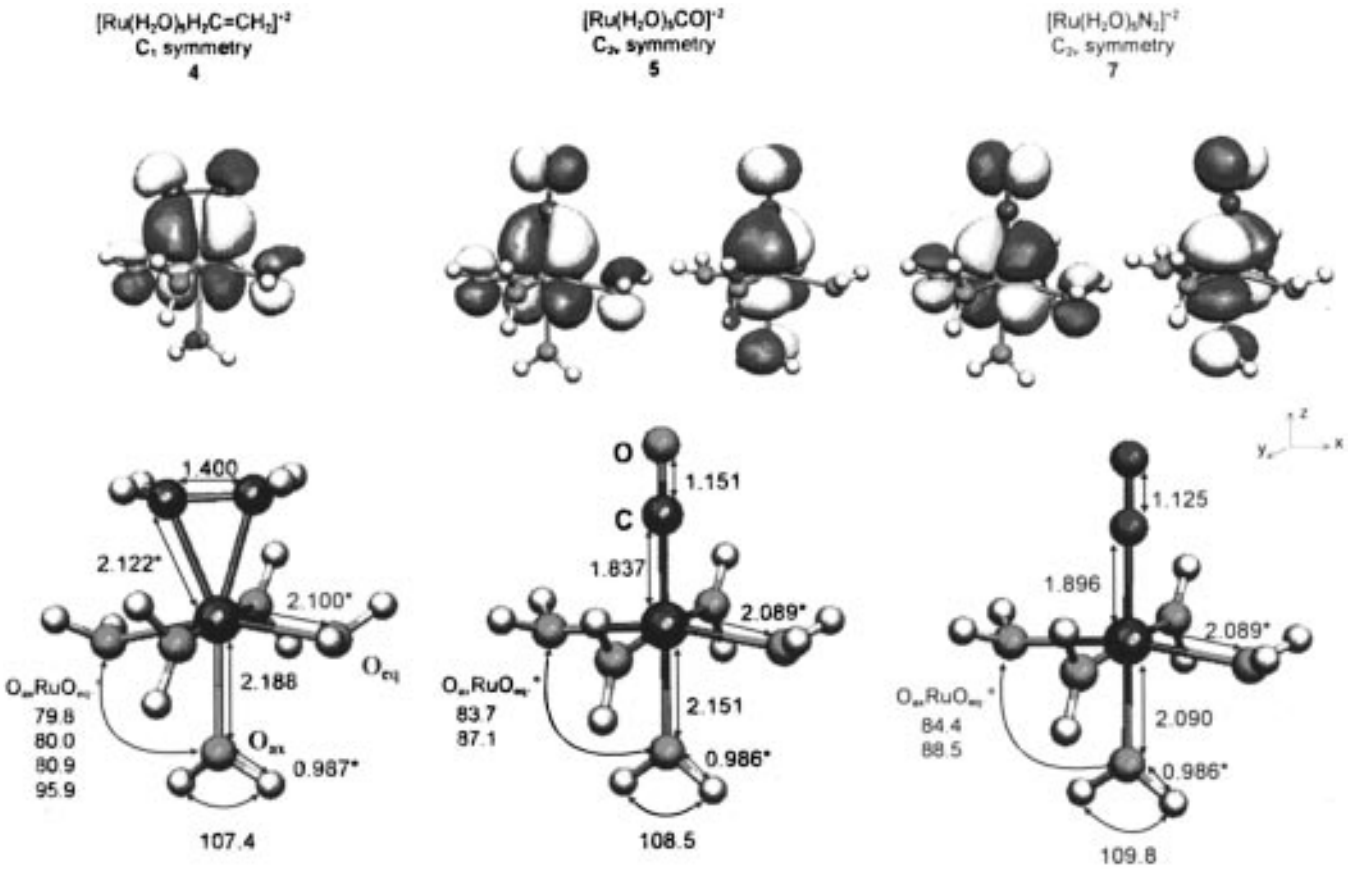

Figure 7. Calculated (deMon LDA) geometries of the $[Ru(H_2O)_6]^{2+}$ complexes (L = $H_2C{=}CH_2$, CO, N_2) and three-dimensional models of MOs responsible for π back-bonding of the corresponding systems. Distances are in angstroms and bond angles in degrees (*: average values).

Table 10. Experimental Free Energies of Activation, $\Delta G^{\ddagger}$ (298.15 K), for Water Exchange, Calculated Binding Energies, E_b, and Bond Distances, d, for $[Ru(H_2O)_5L]^{2+}$ Complexes (L = H_2O, $H_2C{=}CH_2$, CO, N_2)

	Ru−H_2O_{ax} bond			Ru−L bond
L (complex)	E_b/kJ mol^{-1}	$\Delta G^{\ddagger}$/kJ mol^{-1}	d/Å	E_b/kJ mol^{-1}
$H_2C{=}CH_2$ (**4**)	166.2	70.4	2.188	248.6
H_2O (**1**)	179.4	83.0	2.095	179.4
CO (**5**)	182.5	81.0[a]	2.151	286.4
N_2 (**7**)	208.5	99.1[b]	2.090	188.3

[a] Evaluated from the value at 279.4 K using $\Delta H^{\ddagger}$ = 85.2 kJ/mol (see ethylene complex). [b] Value for the dissociation of the Ru−N_2 bond.

consider that the redox potential reflects the electronic density on the metal, the two linear relationships describe the increase of the deshielding on the oxygen atom of the water molecules with the increase of the positive charge on the metal.

Mechanism of the Water Exchange Reaction. The mechanism of the substitution reactions of $[Ru(H_2O)_6]^{2+}$ has been determined by comparing the rate constants for the monocomplex formation between this aqua ion and different ligands.[45] The extreme similarities between the inner sphere interchange rate constants, k_I, led the authors to assign a dissociative interchange mechanism, I_d. The large diversity of the ligands used in this previous study left little doubt about this assignment in spite of the fact that the volume of activation for the water exchange on $[Ru(H_2O)_6]^{2+}$ was found to be close to zero ($\Delta V^{\ddagger}$/cm^3 mol^{-1} = −0.4).[44]

The activation volumes measured for the exchange of the axial and equatorial water molecules ($\Delta V^{\ddagger}$/cm^3 mol^{-1} = +6.5 and +6.1, respectively) are noticeably more positive than in the case of the hexaaqua complex. These differences may result from the increase in the dissociative character of the two exchange reactions taking place in the case of the monocomplex with ethylene. Whether the mechanism should be assigned as dissociative, D, or interchange dissociative, I_d, in these cases cannot be settled definitely on the basis of $\Delta V^{\ddagger}$ values alone. However, the value of +6.5 cm^3 mol^{-1} is, to our knowledge, the most positive one measured for a water exchange reaction on a metal with a d^6 low-spin configuration and must be considered as reflecting the strong dissociative character of the mechanism. This conclusion is supported by the large and positive values of the entropies of activation measured in this study (Table 3). It is to be noticed that the activation volumes are identical for the axial and equatorial exchange reactions, even though the reactivity is quite different for the two sites. In particular, the exchange of the axial water in **4** is more than 2 orders of magnitude faster than the water exchange in $[Ru(H_2O)_6]^{2+}$ whereas the exchange of the equatorial water is 2 orders of magnitude slower.

It must be stressed that the above mechanistic assignment is different from the one operating in the case of the square planar complexes of platinum(II) or palladium(II), with which most of the articles concerning the kinetic *cis* and *trans* effects deal. For these two metal ions, an associative mechanism, A, operates for the substitution reactions, in the absence of peculiar conditions.[52] During the association, the transition state is characterized by an increase of the electronic density around the cation due to the approach of the incoming ligand. Thus, one model used to rationalize the kinetic *trans* effect exercised by π-acceptor ligands like ethylene or CO is based on the stabilization of the transition state by transfer of the excess of electronic density from the metal to the empty π orbitals of the

(52) Romeo, R. *Comments Inorg. Chem.* **1990**, *11*, 21.

Table 11. Comparison of the Water Exchange Rate Constants, of the Redox Potentials, and of the ^{17}O Chemical Shifts for the Complexes of $[Ru(H_2O)_5L]^{2+}$

	H_2O	MeCN	Me_2SO	$H_2C{=}CH_2$	N_2	CO	$F_2C{=}CH_2$	COD[a]
$E^{\circ\prime}$ or E_p[b]/V vs NHE	0.20	0.46	0.81	0.83	0.92	1.09	1.16	
E_{calc}[c]/V vs NHE	−0.08	0.27	0.41	0.74	0.65	1.01		
k_{ax}^{279}/s^{-1}	1.5×10^{-3} (k_{ex})	3.9×10^{-4}	6.8×10^{-2}	0.26		3.8×10^{-3}	0.56	4.6×10^{-2}
k_{eq}^{298}/s^{-1}	1.8×10^{-2} (k_{ex})	1.5×10^{-3}	1.9×10^{-5}	2.8×10^{-4}		2.9×10^{-6}	9.3×10^{-6} (308.4 K)	1.5×10^{-5}
k_{ax}/k_{ex} (279 K)	1	0.26	45	173		2.5	373	31
$_{keq}/k_{ex}$ (298 K)	1	0.083	0.0011	0.016		0.000 16	0.000 15[d]	0.0008
δ_{ax}/ppm	−192	−115	−58	−47	−86	−29	−31	−64
δ_{eq}/ppm	−192	−179	−164	−160	−165	−155	−147	−118

[a] Reference 65. [b] $(E_p^a + E_p^c)/2$ for reversible processes and E_p^a at 0.20 V s^{-1} for chemically irreversible processes. [c] Calculated according to the method described by Lever.[51] [d] 308.4 K.

ligand.[53] However, such an explanation is not valid to rationalize the *cis* and *trans* effects in the octahedral Ru(II) complexes studied here, for which bond breaking is rate determining. The effects of L on the equatorial and axial positions are quite different and will be discussed separately.

Effect of L on the Reactivity of the Equatorial Water Molecules. The *cis*-effect series can be summarized as follows, where k_{ex} is the water exchange rate constant in $[Ru(H_2O)_6]^{2+}$:

	$F_2C{=}CH_2$	~	CO	<	Me_2SO	<	N_2	<	$H_2C{=}CH_2$	<	MeCN	<	H_2O
k_{eq}/k_{ex}	0.0002		0.0002		0.001		0.0016		0.02		0.08		1

N_2 has been included in this series even though the water exchange reactions depend on the dissociation of the Ru−N_2 bond and not directly on the lability of the *cis* and *trans* water molecules. In fact, the value reported in the series above for the dinitrogen complex represents the upper limit of the rate of exchange of the equatorial water, as these molecules are less labile than dinitrogen (vide infra). In Figure 8 are reported the water exchange rate constants measured at 298 K as a function of the redox potentials listed in Table 1. A reasonably good linear dependence is observed between the two parameters. This type of relationship has already been reported many times in the literature, notably to rationalize the *cis*[54] and *trans*[55] $[Ru^{II}(NH_3)_4P(III)(H_2O)]^{2+}$ complexes. The increase of the Ru(III) character of the metal center, reflected in the increase of the redox potential, $E^{\circ\prime}$, was used to explain the lability of the water molecule,[55] as Ru(III) is known to be less reactive than Ru(II).[44]

Despite the large range of reactivities exhibited by the equatorial water molecules, the Ru−O_{eq} bond distances calculated for **4**, **5**, and **7** (Figure 7) lie close to the Ru−O bond length calculated for the hexaaqua ion (2.095 Å). The fact that no shortening of the Ru−O_{eq} bonds with a decrease of the lability is observed may be due to the great compactness of **1**, as is expected for a d^6 low-spin complex. This has already been observed in the case of $[Rh(H_2O)_6]^{3+}$, another d^6 low-spin complex, where an important crystal field stabilization argument was used to explain the abnormally small partial molar volume of this aqua ion.[56] The effect of L on the stability of the transition state may also play an important role in the lability of the water molecules. This may possibly be more important than the effects on the ground state and explain why no difference in bond lengths is calculated for the Ru−O_{eq} bonds.

Effect of L on the Reactivity of the Axial Water Molecule. The series of increasing *trans* effect of L in $[Ru(H_2O)_5L]^{2+}$ is as follows:

	N_2	<<	MeCN	<	H_2O	<	CO	<	Me_2SO	<	$H_2C{=}CH_2$	<	$F_2C{=}CH_2$
k_{ax}/k_{ex}	0.0015		0.3		1		2.5		45		173		373

As can be seen in Figure 8, the reactivity of the *trans* water molecule can no longer be linearly related to the redox potential of the corresponding complex. The *trans*-labilizing effect exhibited by π-acceptor ligands has already been mentioned previously for complexes of the type *trans*-$[Ru(NH_3)_4L(H_2O)]^{2+}$, where L = SO_3^{2-}, CN^-, and C-bonded imidazole.[57] However, no satisfactory explanation could be given. Some authors tentatively tried to attribute these effects to substantial σ overlap between the π-acceptor ligands and the metal.[58] For *trans*-$[Ru(NH_3)_4L(H_2O)]^{2+}$, the two slowest water exchanges were reported for L = CO and N_2 by Taube et al.[57] Comparatively, the exchange of the water *trans* to CO was at least 10^6 times slower than when it was *trans* to a purely σ-donating ligand like ammonia.[57,59]

We can use the results obtained by DFT calculations to better understand the observed labilizing effects. When the calculated Ru−O_{ax} bonding energies, E_b, are compared with the $\Delta G^{\ddagger}$ free energies of activation for water exchange reported in Table 10, it is seen that a good correlation appears between these properties: the less labile Ru−O_{ax} bond in **7** corresponds to a comparatively important increase of E_b, and, inversely, the labile Ru−O_{ax} bond in **4** is reflected in a small bonding energy. The *trans* effects of H_2O and CO are quite similar (Table 11), and this corresponds to similar E_b values. This means that increasing bonding energies correspond to increasing activation energies of the axial ligand, even though entropy effects are not included in calculations of bonding energies. This might indicate that entropy contributions to $\Delta G^{\ddagger}$ should remain essentially constant along the series **4**, **1**, **5**, **7**. However, the correlation between the calculated binding energies of the axial water and the optimized Ru−O_{ax} bond distances (Table 10) and, de facto, between the $\Delta G^{\ddagger}$ values and the distances is not as good. Even though the ordering of the systems is the same for these two parameters, a strong difference in lability between **1** and **7** corresponds to a small difference in bond length, whereas a very small lability difference, such as that between **1** and **5**, corresponds to an important disparity in the bond lengths. This might be due to the fact that the large differences (up to 25%) in binding energies correspond to small differences (4%) in bond lengths, and it is consequently difficult to correlate energies and structural parameters exhibiting variations differing by 1 order of magnitude. It is reassuring that the calculated 8.5 pm excess *trans* versus *cis* Ru−OH_2 bond length for **5** is in good agreement with that of 6.3 pm found in the X-ray structure of [(COD)-$Ru(H_2O)_4$](OTs)$_2$.[6a]

(53) Tobe, M. L. *Inorganic Reaction Mechanisms*; Nelson: Nairobi, Kenya, 1992.
(54) Leising, R. A.; Ohman, J. S.; Takeuchi, K. J. *Inorg. Chem.* **1988**, *27*, 3804.
(55) do Nascimento Filho C.; de Lima, J. B.; dos Santos Lima Neto, B.; Franco, D. W. *J. Mol. Catal.* **1994**, *90*, 257.
(56) Swaddle, T. W.; Mak, M. K. Can. J. Chem. **1983**, 61, 473.
(57) (a) Isied, S.; Taube, H. *Inorg. Chem.* **1974**, *13*, 1545. (b) Isied, S.; Taube, H. *Inorg. Chem.* **1976**, *15*, 3070.
(58) Allen, R. J.; Ford, P. C. *Inorg. Chem.* **1974**, *13*, 237.
(59) Bernhard, P.; Lehmann, H.; Ludi, A. *Comments. Inorg. Chem.* **1983**, *2*, 145.

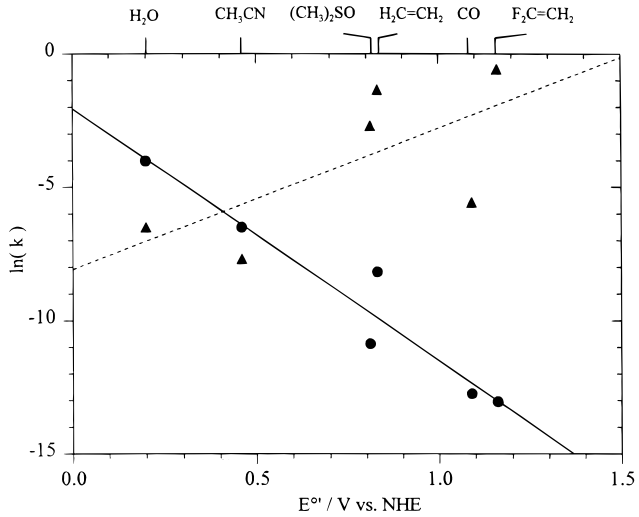

Figure 8. Plot of the natural logarithm of the rate constant for the exchange of the axial (▲, $T = 279$ K) and equatorial (●, $T = 298$ K) water molecules in the complexes $[Ru(H_2O)_5L]^{2+}$ as a function of $E^{\circ\prime}$. The value k_{eq}^{298} for L= $F_2C{=}CH_2$ was extrapolated from the measured value at 308 K using $\Delta H_{eq}^{\ddagger} = 106.6$ kJ mol^{-1}of $[Ru(H_2O)_5(H_2C{=}CH_2)]^{2+}$.

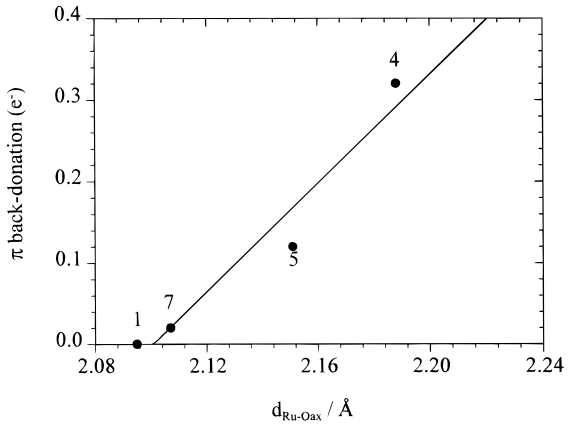

Figure 9. π back-bonding electron transfer to the ligand L in $[Ru(H_2O)_5L]^{2+}$, L = H_2O (**1**), $H_2C{=}CH_2$ (**4**), CO (**5**), and N_2 (**7**), represented as a function of the calculated Ru−O_{ax} bond lengths.

Further, it is interesting to calculate the amount of π back-bonding electron transfer to the L ligand for the various systems, by using the charge distribution of the predominantly 4d MOs. This calculation leads to the following values: 0.0 e for **1**, 0.02 e for **7**, 0.12 e for **5**, and 0.32 e for **4**, which correlate fairly well with the Ru−O_{ax} bond distances (Figure 9). Clearly, this should be interpreted in terms of the well-known *trans* influence: the axial H_2O ligand in the *trans* position with respect to L exhibits a Ru−O_{ax} bond length which is much more sensitive to the nature of L than the equatorial ones. In particular, the Ru−O_{ax} bond distance increases most for complexes in which there is the largest π back-donation toward L, as such a donation is performed at the expense of the σ-bonding electrons located in the Ru−O_{ax} bond.

Finally, Figure 10, which displays the calculated electron density contours of **1** and **4**, allows us to conclude indeed that the σ-bonding electron density in the Ru−O_{ax} region is significantly smaller for **4** than for **1**, which is the origin of the longer Ru−O_{ax} bond length in **4**.

Water Exchange in $[Ru(H_2O)_5N_2]^{2+}$. The behavior of **7** is a peculiarity among the Ru(II) compounds studied. As can be seen in Table 10, this is the only case where the binding energy between the metal and L is lower than that between Ru and the water molecules of the first coordination sphere. This led us

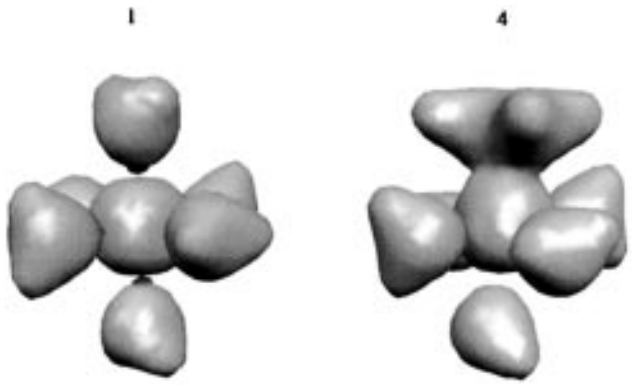

Figure 10. Three-dimensional models of calculated electron densities of $[Ru(H_2O)_6]^{2+}$ (**1**) and $[Ru(H_2O)_5(H_2C{=}CH_2)]^{2+}$ (**4**) (isosurface value: 0.08 au).

Scheme 4. Reaction Pathways for the Formation of the $[\{Ru(H_2O)_5\}_2N_2]^{4+}$ Dimer and for the Water Exchanges on $[Ru(H_2O)_5N_2]^{2+}$ Where the Rate-Determining Step is the Dissociation of the Ru−O_{ax} Bond (a) and Where It Is the Dissociation of the Ru−N_2 Bond (b)

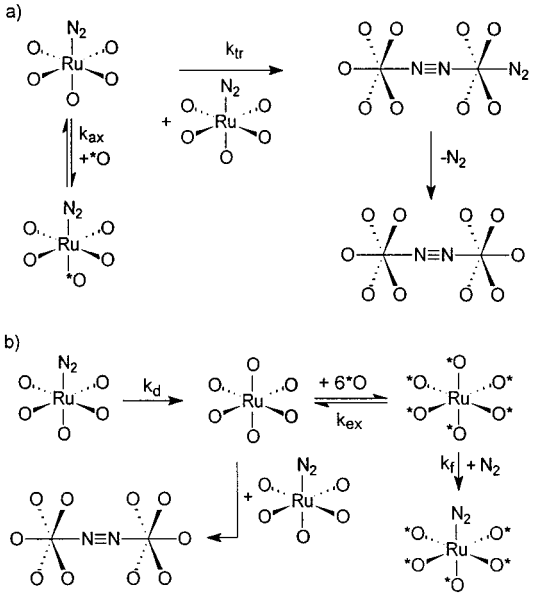

to develop the kinetic model, expressed by eqs 16−19, to describe the water exchanges in the dinitrogen complex (Scheme 3). Several experimental observations confirm the choice of this reaction pathway over a direct exchange between the water molecules in **7** and the bulk as depicted in Scheme 2. First, the equatorial and axial water exchange rate constants are equal. This is understood in Scheme 3, as the rate-determining step (rds) is common for the two exchanges, i.e. the dissociation of the Ru−N_2 bond. This dissociation leads to the formation of **1**, where the distinction between axial and equatorial positions is removed. The other argument confirming our hypothesis is the observation of the dimerization of **7** to form $[\{Ru(H_2O)_5\}_2N_2]^{4+}$, where two Ru(II) centers are bridged by one dinitrogen molecule.[7] In the absence of dinitrogen pressure, this dimerization is observed in parallel at a rate similar to that of the water exchanges. The two possible reaction pathways envisaged here for the water exchange on **7** and for the formation of the dimer are shown in Scheme 4. Scheme 4a is the hypothesis where the axial water exchanges directly with the bulk and where the dimer is formed by reaction between two $[Ru(H_2O)_5N_2]^{2+}$ complexes. In the hypothesis of a dissociative mechanism, which seems the rule for the ruthenium(II) aqua complexes, the rate of formation of the dimer would depend

on the reactivity of the axial water molecule in **7**. In the case of the Eigen−Tamm−Wilkins mechanism,[60] the second-order rate constant for the formation of the dimer, k_f, can be decomposed into an equilibrium constant for the formation of an outer-sphere complex, K_{os}, and the first-order rate constant, evaluated here as the axial water exchange rate constant, $k_f = fK_{os}k_{ax}$, where f is a statistical factor, which is smaller than 1, describing the probability of replacement of the leaving water by one peculiar ligand of the second coordination sphere and which is neglected. K_{os} for the reaction between a dipositive cation and a positively charged ligand has been estimated as 0.02[61] and can be taken as an upper limit in our case.[62] If we take the value of 2.9×10^{-5} s^{-1} for k_{ax}, we obtain k_f/mol^{-1} kg s^{-1} $= 0.02 \times 2.9 \times 10^{-5} = 5 \times 10^{-7}$. For a concentration in monocomplex of 0.1 mol kg^{-1}, this corresponds to a half-time of more than 3 months (lower limit). Consequently, if Scheme 4a would apply, the dimer could not appear at rates comparable to that of the water exchange. On the contrary, if Scheme 4b applies, the rate-determining step for the water exchange and for the dimerization is the loss of the dinitrogen molecule, as the intermediate formed (**1**) is more than 600 times more reactive than the starting material. All the above observations allow us to conclude that the proposed reaction pathway for the water exchanges on **7** (Scheme 3) is effectively the one that takes place.

It has been noted that the product of the reaction of *cis*-$[Ru(NH_3)_4(N_2)H_2O]^{2+}$ with isonicotinamide (isn) is in fact the bis(isonicotinamide) complex.[57] The appearance of this biscomplex was explained by the weakening of the $Ru^{II}-N_2$ bond after the replacement of H_2O by the π acid isn. According to the relative stability of the $Ru^{II}-N_2$ and $Ru^{II}-H_2O$ bonds observed in our studies, it may be that the replacement of N_2 by the isn ligand occurs before the substitution of the water molecule.

We have shown that the rate constant, k_f, for the reaction between $[Ru(H_2O)_6]^{2+}$ and L does not depend on the nature of L.[45] Consequently, it is possible to estimate the equilibrium constant, $K_{eq} = k_f/k_d$, for the formation of the dinitrogen monocomplex. The calculations give the value of $K_{eq} = 2.1 \times 10^{-3}/2.9 \times 10^{-5} = 72$ mol^{-1} kg. This value is considerably smaller than the corresponding one found for the reaction $[Ru(NH_3)_5H_2O]^{2+} + N_2 = [Ru(NH_3)_5N_2]^{2+} + H_2O$, where $K_{eq} = 3.3 \times 10^4$ M^{-1}.[63] It appears from these results that the $Ru^{II}-N_2$ bond is more stable when it is *trans* to an N-bonded ligand like ammonia than when it is *trans* to an O-bonded one like water.

Concluding Remarks. It is important to stress that a perfect understanding of the *cis* and *trans* effects in complexes with octahedral geometry is far from being completely achieved. Even in the case of square-planar complexes, on which most of the work in this field has concentrated, these phenomena are still subject to discussion. A recent paper,[64] attributing the trans effect of pure σ-donating ligands to transition state effects rather than to ground state effects, as commonly believed previously, demonstrates the controversy in this area. The octahedral case appears even more difficult to rationalize, as a greater diversity of mechanism, lability, and chemical properties is found for this type of geometry. Usually, a ligand series of increasing *trans* effect determined for a particular type of complex is not transferable to other complexes, and trying to build a universal series of ligands, according to their labilizing properties, that can rationalize all the observed effects, lamentably fails. Effects such as the nature of the metal center, the mechanism of the substitution reactions, the nature of the leaving group and in particular its σ- and π-bonding properties, and steric effects have to be taken into account when creating this type of series. Even for similar systems like $[Ru(H_2O)_5L]^{2+}$ and *trans*-$[Ru(NH_3)_4L(H_2O)]^{2+}$, the labilizing effects are not transposable.[57]

We can assert that only a thorough knowledge of the electron distribution among the different bonds of a complex, of the energy of the orbitals involved in the bonds, and of the structure of the complexes can lead us to a better understanding of the labilizing effects taking place in the first coordination sphere in an octahedral geometry. In that respect, computational calculations are among the most powerful tools to estimate these different parameters. In our case, the calculations gave us a better description of the electron distribution among the Ru−ligand bonds. Due to the lack of crystallographic structures, they also provided the only method to evaluate the possible correlation between the reactivities and the lengths of the Ru−OH_2 bonds. But, most importantly, they allowed us to recognize the weakest bond in the complexes, through the calculation of some bond energies. In the case of $[Ru(H_2O)_5N_2]^{2+}$, the Ru−N_2 bond was shown to be weaker than the Ru−OH_2 bonds, and this led us to establish the reaction pathway depicted in Scheme 3, which was then checked and confirmed by the experimental observations.

Acknowledgment. The authors thank the Swiss National Science Foundation for financial support (Grant 2-45419.95) and Dr. Urban Frey for his assistance and for useful discussions.

Supporting Information Available: Initial reactant concentrations, ionic strength, and rate constants as a function of pressure for the exchange reaction of the equatorial water molecules in $[Ru(H_2O)_5(H_2C{=}CH_2)]^{2+}$ (Table S1), initial reactant concentrations and transverse relaxation rate, $1/T_2{}^b$, as a function of temperature of the ^{17}O NMR signal of the axial water molecule in $[Ru(H_2O)_5(H_2C{=}CH_2)]^{2+}$ and in $[Ru(H_2O)_5(FC{=}CH_2)]^{2+}$ (Tables S2 and S3), and the mathematical development of eqs 12−15 and eqs 16−19 (9 pages). Ordering information is given on any current masthead page.

IC970783Y

(60) (a) Eigen, M.; Tamm, K. Z. *Elektrochem.* **1962**, *66*, 93. (b) Wilkins, R. *Acc. Chem. Res.* **1970**, *3*, 408.
(61) Burgess, J. *Metal Ions in Solution*; Ellis Horwood Limited: Chichester, U. K., 1978; Chapter 12 and references therein.
(62) The validity of the "ion-pair model" with such a small outer-sphere equilibrium constant could be questioned; however, the value taken here is certainly good as an upper limit and describes the difficulty of encounter between two dipositive cations.
(63) Armor, J. N.; Taube, H. *J. Am. Chem. Soc.* **1970**, *92*, 6170.
(64) Lin, Z.; Hall, M. B. *Inorg. Chem.* **1991**, *30*, 646.
(65) Dadci, L. University of Lausanne. Personal communications.